

## Supporting Information

### Layer-by-layer assembling $\text{Cu}_3(\text{BTC})_2$ on chitosan non-woven fabrics: A promising haemostatic decontaminant composite materials against sulfur mustard

*Lijuan Zhang,<sup>a</sup> Junmei Sun,<sup>a</sup> Yunshan Zhou,<sup>\*a</sup> Yuxu Zhong,<sup>\*b</sup> Ying Ying,<sup>b</sup> Yanqin Li,<sup>a</sup>*

*Hongyan Liu,<sup>b</sup> Yanqin Liu,<sup>b</sup> Zareen Zuhra<sup>a</sup> and Chunqian Huang<sup>b</sup>*

<sup>a</sup>Resource Engineering, Institute of Science, Beijing University of Chemical Technology, Beijing 100029, P. R. China; <sup>b</sup>State Key Laboratory of Toxicology and Medical Counter measures, Beijing Institute of Pharmacology and Toxicology, Beijing 100850, P. R. China.

E-mail: zhouys@mail.buct.edu.cn (Y. Zhou); yuxuzhong2008@aliyun.com (Y. Zhong)

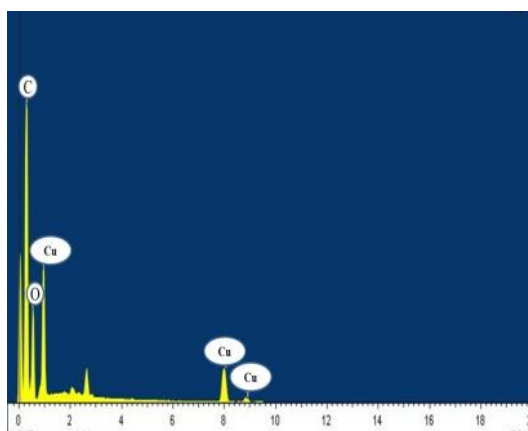


**Figure S1.** EDX images of  $[\text{Cu}_3(\text{BTC})_2]_4@$ chitosan showing presence of the constitute elements C, O and Cu.

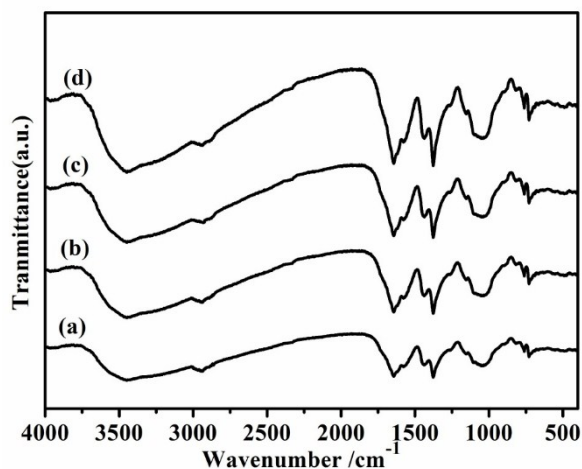


**Figure S2.** IR spectra of  $[\text{Cu}_3(\text{BTC})_2]_n@$ chitosan fibers with  $n = 2$  (a), 4 (b), 6 (c), and 8 (d).

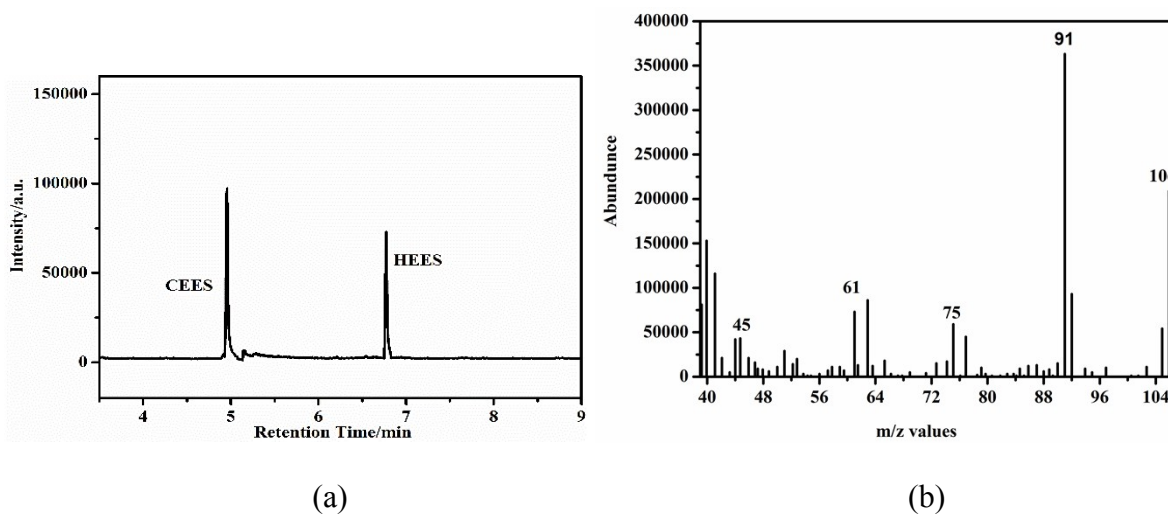


**Figure S3.** GC-MS data showing the formation of hydroxyl ethyl ethyl sulphide: GC spectrum (a) and MS spectrum of hydroxyl ethyl ethyl sulphide (b).

As shown in Figure S3, because of the high toxicity of HD, we used its monofunctional analog 2-chloroethyl ethyl sulfide (CEES) to identify the mechanism of degradation by  $[\text{Cu}_3(\text{BTC})_2]_4@$ chitosan. The GC-MS data indicates that the m/z values at



**Figure S5.** Histological examination of  $\text{Cu}_3(\text{BTC})_2$  toxicity on mice heart (hematoxylin eosin dyeing,  $\times 20$ ): Control group (a);  $\text{Cu}_3(\text{BTC})_2$  1 mg/kg group (b);  $\text{Cu}_3(\text{BTC})_2$  10 mg/kg group (c);  $\text{Cu}_3(\text{BTC})_2$  50 mg/kg group (d).

As with the control group (Figure S5a), there was dilation and congestion in myocardial interstitial vascular, mild degeneration and hyperemia in myocardial cells, and no hemorrhage and myocardial necrosis were observed (Figure S5b – 5d) for the  $\text{Cu}_3(\text{BTC})_2$ -treated groups, i.e., no significant difference in lesions and morphological changes between  $\text{Cu}_3(\text{BTC})_2$  treated groups and normal control group were observed.

#### **Toxicity results of hepatic tissues**

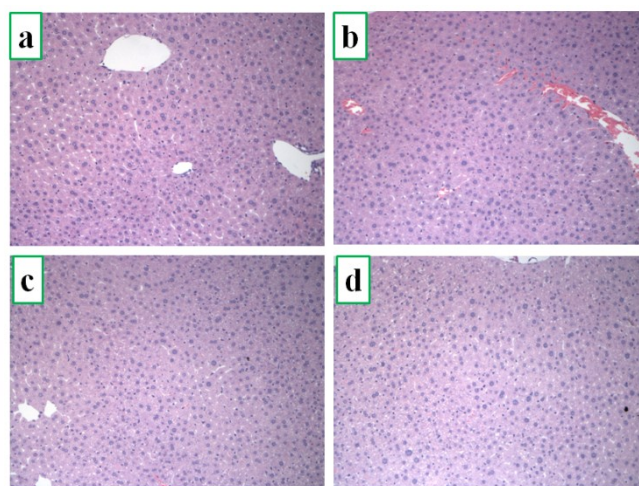


**Figure S6.** Histological examination of  $\text{Cu}_3(\text{BTC})_2$  toxicity on mice liver (hematoxylin eosin dyeing,  $\times 20$ ): Control group (a);  $\text{Cu}_3(\text{BTC})_2$  1 mg/kg group (b);  $\text{Cu}_3(\text{BTC})_2$  10 mg/kg group (c);  $\text{Cu}_3(\text{BTC})_2$  50 mg/kg group (d).

As shown in Figure S6a, the micrograph of the control sections of the liver tissue showed normal histological features with the hepatic lobules showing irregular hexagonal

boundary defined by portal tract and sparse collagenous tissues. The hepatic portal veins, bile ductles and hepatic artery within the portal tract were all visible. It was found that no significant differences existed with regards to the total hepatocyte number and their numerical density between  $\text{Cu}_3(\text{BTC})_2$  treated groups (Figure S8b-8d) and the control group.

### Toxicity results of spleen tissues

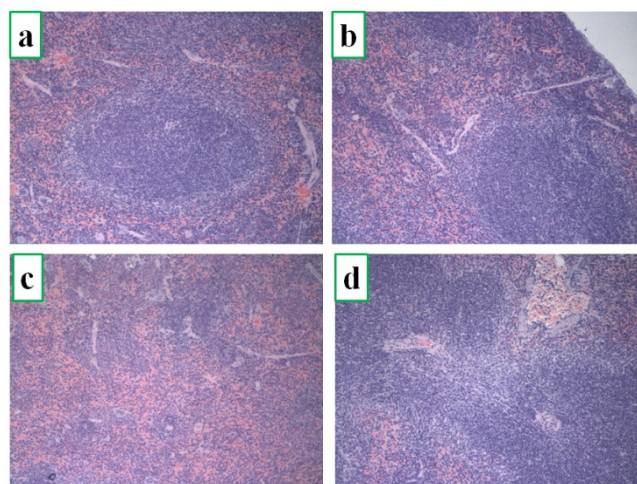


**Figure S7.** Histological examination of  $\text{Cu}_3(\text{BTC})_2$  toxicity on rat spleen (haematoxylin eosin dyeing,  $\times 20$ ): Control group (a);  $\text{Cu}_3(\text{BTC})_2$  1 mg/kg group (b);  $\text{Cu}_3(\text{BTC})_2$  10 mg/kg group (c);  $\text{Cu}_3(\text{BTC})_2$  50 mg/kg group (d).

As shown in Figure S7a, white pulp of lymphoid tissue in the control group composed of PALS (periarterial lymphoid sheath) and lymph follicle were clearly seen. The PALS was composed of central region, the peripheral region, and the marginal zone bridging channel. The lymphocytes which proliferated to external fringes were surrounded by red pulp. The red pulp possessed medullary sinus filled with red blood cells. Compared with

control group, no significant changes were observed on the splenic corpuscle, germinal center, PLAS and the marginal zone of  $\text{Cu}_3(\text{BTC})_2$  treated groups (Figure S7b-S7d).

### Toxicity results of lung tissues

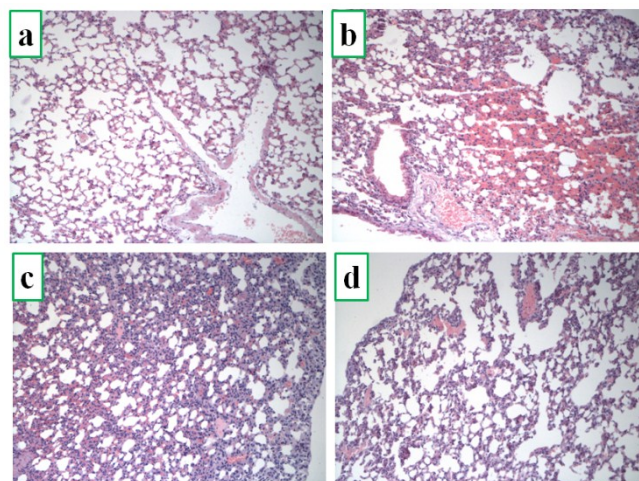


**Figure S8.** Histological examination of  $\text{Cu}_3(\text{BTC})_2$  toxicity on rat lung (hematoxylin eosin dyeing,  $\times 20$ ): Control group (a);  $\text{Cu}_3(\text{BTC})_2$  1 mg/kg group (b);  $\text{Cu}_3(\text{BTC})_2$  10 mg/kg group (c);  $\text{Cu}_3(\text{BTC})_2$  50 mg/kg group (d).

As compared with the control group, histological abnormalities were limited mostly to inflammatory cells infiltration and broadened alveolar walls in  $\text{Cu}_3(\text{BTC})_2$  treated groups (Figure S8). The effect was dose-dependent since moderate pneumonia was found in animals exposed to the high dose of  $\text{Cu}_3(\text{BTC})_2$ .

### Toxicity results of renal tissues

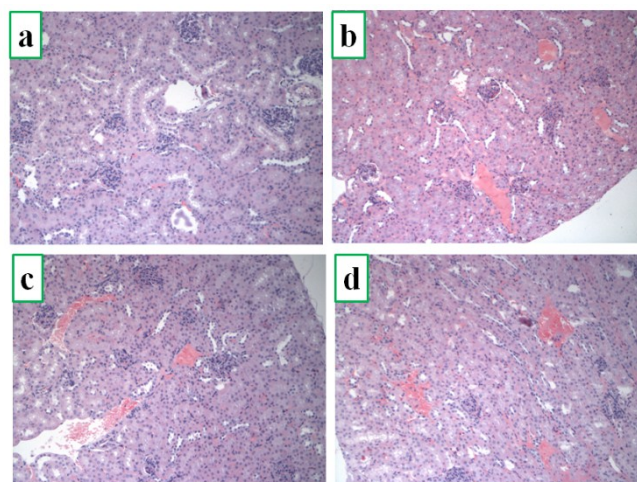


**Figure S9.** Histological examination of  $\text{Cu}_3(\text{BTC})_2$  toxicity on rat kidney (hematoxylin eosin dyeing,  $\times 20$ ). Control group (a);  $\text{Cu}_3(\text{BTC})_2$ , 1 mg/kg group (b);  $\text{Cu}_3(\text{BTC})_2$ , 10 mg/kg group (c) and  $\text{Cu}_3(\text{BTC})_2$ , 50 mg/kg group (d).

As shown in Figure S9, the nuclear characteristics, morphological features, and tissue integrity of kidney of the  $\text{Cu}_3(\text{BTC})_2$  treated group were essentially normal and comparable to the control. However, mild capillary hyperemia and occasional bleeding can be seen in the  $\text{Cu}_3(\text{BTC})_2$  treated group.

### **Preparation of the standard solution of HD**

The concentration of sample was determined below. In brief,  $5\mu\text{l}$  of HD was dissolved in petroleum ether to prepare a standard HD solution (1 mg/mL) for determining HD absorbance. The standard HD solution was diluted to various concentrations by addition of desired amount of petroleum ether (Table S1). Afterwards,  $200\mu\text{l}$  of alkalized thymol phthalate blue T135 (denoted as the blue reagent for short) and  $100\mu\text{l}$  of absolute ethyl alcohol was added to the solutions. The blue reagent used in this work was prepared as

follows: 0.2 g of NaOH and 1.2 g of thymolphthalein was dissolved in a solution containing 12.5 ml of H<sub>2</sub>O and 87.5 ml of anhydrous ethanol.

**Table S1.** Preparation of the standard solution of HD of different concentrations

Number	Standard HD solution (μL)	Petroleum ether (μL)	The blue reagent (μL)	Absolute ethyl alcohol (μL)
1	0	100	200	100
2	20	80	200	100
3	40	60	200	100
4	60	40	200	100
5	80	20	200	100
6	100	0	200	100

The HD solution of different concentrations (Table S1) was heated at 80 °C in water bath, followed by addition of 5 μL of 6 mol/L acetic acid and 3 mL 95% ethanol. The colors of the resulting solutions are shown in Figure S10.



**Figure S10.** The colors for different concentrations of HD solution containing acetic acid and ethanol (No.1-No.6 from left to right)

### Calibration curve for the determination of HD

The standard solutions **1 – 6** of HD show a UV–visible absorption peak at about 447 nm (Figure S11). In order to get calibration curve for the determination of HD, absorbance ( $\lambda_{\text{max}} = 447 \text{ nm}$ ) was plotted against the concentration of HD. Thus, the calibration curve was acquired with the regression equation  $y = 0.128 + 0.0847x$  where  $y$  is the absorbance value and  $x$  is the residual concentration with a correlation coefficient of  $R^2 = 0.993$ .

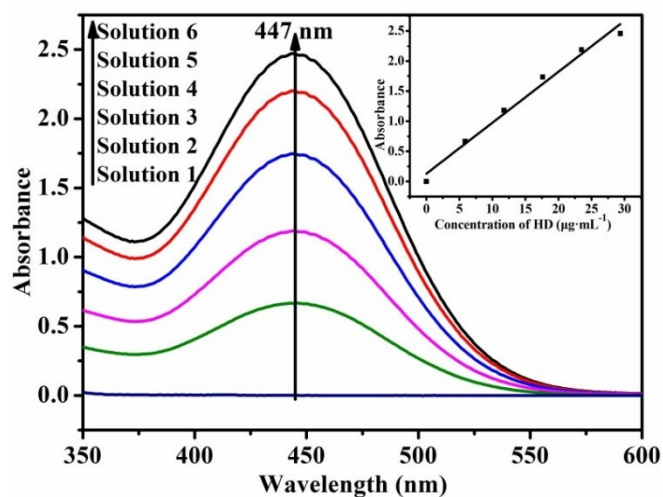


**Figure S11.** UV-vis absorbance curve of HD solutions of different concentration. Insert images are absorbance value of solution at 447 nm vs. concentration of HD.

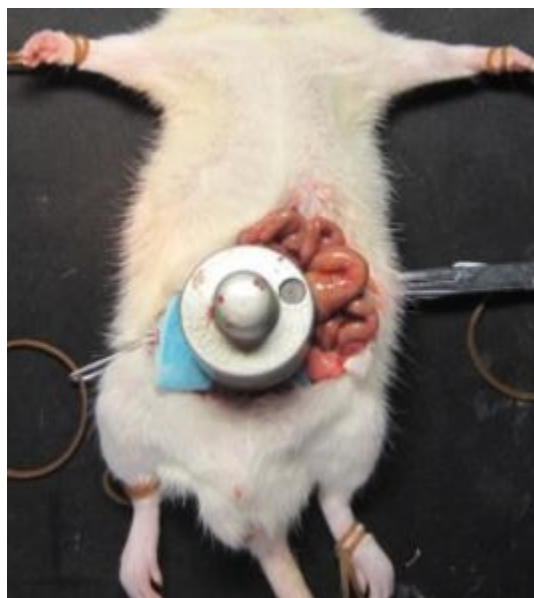


**Figure S12.** Photographic image of wound model using a Wistar rat.

**Table S2.** Decontamination efficiency of HD and its analogue on different materials

Materials	The amount of detergent/mg	The amount of HD/CEES / $\mu$ l	Decontamination time /h	Rate /%	Reference
10% $H_4PVMo_{11}O_{40}$ /Carbon	100	1 (HD)	48	91	[s1]
ylon-6/ $H_6PV_3Mo_9O_{40}$	150	5 (HD)	6	41.55	[s2]
10% $H_6PV_3Mo_9O_{40}/Al_2O_3$	100	5 (HD)	6.7	58.52	[s3]
MgO/C-1	50	2 (CEES)	5	86	[s4]
$K_5[(Fe^{III}(OH)_2)_3(A-\alpha-PW_9O_{34})_2]/(Si/AlO_2)$	25	6 (CEES)	20	94	[s5]
Montmorillonites/ $Ag_2O$	500	5 (HD)	2	100	[s6]
CuO	100	5 (HD)	24	96.2	[s7]
MgO	150	5 (CEES)	24	84	[s8]
hydrogen peroxide /Activated Carbon	40	1.6 (HD)	48	97	[s9]
$Ce_{0.5}Zr_{0.5}O_2$	100	5 (CEES)	7.5	85	[s10]

Copper acetate	50	5 (HD)	3	6	[s11]
[Cu <sub>3</sub> (BTC) <sub>2</sub> ] <sub>4</sub>	50	5 (HD)	0.67	70	[s11]
[Cu <sub>3</sub> (BTC) <sub>2</sub> ] <sub>4</sub> @chitosan	15	4 (HD)	0.5	86	this work

## Reserences

[s1] Sharma A, Singh B, Saxena A. Polyoxometalate impregnated carbon systems for the in situ degradation of sulphur mustard . *Carbon*, 2009, **47(8)**, 1911-1915.

[s2] Liu F, Lu Q, Jiao X, Chen D. Fabrication of nylon-6/POMs nanofibrous membranes and the degradation of mustard stimulant research . *RSC Advances*, 2014, **4(78)**, 41271-41276.

[s3] Saxena A, Singh B, Srivastava A K, Suryanarayana M V S, Ganesan K, Vijayaraghavan R, Dwivedi K K. Al<sub>2</sub>O<sub>3</sub> nanoparticles with and without polyoxometalates as reactive sorbents for the removal of sulphur mustard . *Microporous & Mesoporous Materials*, 2008,**115(3)**, 364-375.

[s4] Vu A-T, Ho K, Lee C-H. Removal of gaseous sulfur and phosphorus compounds by carbon-coated porous magnesium oxide composites. *Chemical Engineering Journal*, 2016, **283**, 1234-1243.

[s5] Guo Y, Wang Y, Hu C, Wang Y, Wang E, Zhou Y, Feng S. Microporous Polyoxometalates POMs/SiO<sub>2</sub>:Synthesis and Photocatalytic Degradation of Aqueous Organochlorine Pesticides . *Chemistry of Materials*, 2000, **12(11)**, 3501-3508.

- [s6] Kumar J P, P.V.R.K R, G.K P, Singh B. Montmorillonites supported with metal oxide nanoparticles for decontamination of sulfur mustard . *Applied Clay Science*, 2015, **116–117**, 263-272.
- [s7] Verma M, Gupta V K, Dave V, Chandra R, Prasad G K. Synthesis of sputter deposited CuO nanoparticles and their use for decontamination of 2-chloroethyl ethyl sulfide (CEES) . *Journal of Colloid and Interface Science*, 2015, **438**, 102-109.
- [s8] Narske R M, Klabunde K J, Fultz S. Solvent Effects on the Heterogeneous Adsorption and Reactions of (2-Chloroethyl)ethyl Sulfide on Nanocrystalline Magnesium Oxide . *Langmuir*, 2002, **18(12)**, 4819-4825.
- [s9] Osovsky R, Kaplan D, Nir I, Rotter H, Elisha S, Columbus I. Decontamination of Adsorbed Chemical Warfare Agents on Activated Carbon Using Hydrogen Peroxide Solutions. *Environmental Science & Technology*, 2014,**48(18)**, 10912-10918.
- [s10] Chen W, Ran R, Weng D, Wu X, Zhong J, Zhu A, Han S. A facile ceria–zirconia binary oxide used for degradation of 2-chloroethyl ethyl sulfide. *Journal of Materials Science*, 2015, **50(19)**, 6268-6276.
- [s11] A. Roy, A. K. Srivastava, B. Singh, T. H. Mahato, D. Shah and A. K. Halve, *Microporous and Mesoporous Mater.* 2012, **162**, 207-212.